ASME Journal of Engineering for Gas Turbines and Power
Online journal at:
https://asmedigitalcollection.asme.org/gasturbinespower

The Role of Part-Load Control Strategies in Optimizing the Efficiency of a Decarbonized Combined Cycle Power Plant in Load-Following Mode

Silvia Ravelli
Department of Engineering and Applied Sciences,
University of Bergamo,
Marconi Street 5,
Dalmine, BG 24044, Italy
e-mail: silvia.ravelli@unibg.it

In pursuit of the goal of decarbonization, postcombustion capture (PCC) by means of monoethanolamine (MEA), exhaust gas recirculation (EGR), and hydrogen cofiring were applied to a 2 × 1 combined cycle (CC) under load-following operation in two typical summer/winter days. Keeping the same electrical demand profiles as in a previous study by the same author, the main novelty is to determine the part-load gas turbine (GT) control strategy that can maximize the CC net electric efficiency ($\eta_{CC,n}$) when applying different decarbonization solutions such as: addition of PCC unit and addition of PCC unit with EGR, when the fuel supply is 100% natural gas (NG) or 65% vol hydrogen cofiring. The multivariable optimization problem, with $\eta_{CC,n}$ as objective function, under the constraint of net power output ($P_{CC,n}$) equal to electricity demand, has been updated to include the following decision variables: load of each GT; EGR rate, depending on the fuel type, i.e., [0; 0.4] for 100% NG versus [0; 0.55] for hydrogen blending; GT inlet air flow and fuel flow, in a range such that the GT outlet temperature is maintained within the limit of about 50 °C above the nominal value. The main finding is that the operating guidelines depend not only on the load but mainly on the environmental conditions. Under hot weather and part-load conditions, the recommendation is to rely on modulating the air/fuel flow at the GT inlet rather than applying EGR. [DOI: 10.1115/1.4069449]

Keywords: combined cycle, load-following, hydrogen, carbon capture, exhaust gas recirculation, part-load control strategy

1 Introduction

Research on the most effective control strategy to optimize part-load performance in conventional heavy-duty combined cycle (CC) units has been extensively covered in published literature. It is well known that the available options are "inlet guide vane (IGV) control" on the one side and "turbine inlet temperature (TIT)/fuel" control on the other side. In the former case the compressor inlet airflow is reduced by closing the IGV, with TIT kept almost constant, thus turbine outlet temperature (TOT) rises. Alternatively, air flow modulation (and fuel control) can keep TOT nearly constant at the design value. In the latter case, the fuel flow is regulated at constant air inlet to reduce TIT, hence TOT. The preferred solution is "IGV control": it ensures higher η_{CC} at part-load because the improvement in Rankine cycle efficiency (η_R) outweighs the decrease in gas turbine (GT) efficiency (η_{GT}), thus shifting power production from the topping to the bottoming cycle [1]. Huang et al. [2] confirmed that IGV plays a role in increasing the steam turbine (ST) power output and reducing the exhaust heat in the heat recovery steam generator (HRSG). Muara Karang CC (block 2) was modeled in Ref. [3]: IGV position was tracked searching for the maximum η_{CC}. The improvement over the existing conditions was significant, up to 1.5% on partial load. Using IGV control to maintain TIT at the design value and then to keep TOT at its maximum value also proved beneficial from a broader point of view, including not only thermodynamic aspects but also economic and environmental ones [4].

Yang et al. [5] combined this control strategy with compressor inlet air heating via part of the HRSG exhaust, which resulted in a further increase in η_{CC} from 1 to 1.7 percentage points (pp), at CC load between 45% and 100%. The heated air entering the GT also increases the HRSG efficiency, according to Wang et al. [6]. In contrast, fuel consumption drops by 0.02/0.03 kg/s at 65/80% CC load, respectively, when it comes to the CC system in Tianjin city (China). Similarly, Varini and Mierka [7] estimated that NG fuel consumption can decrease by 13 m^3/h for each 1 °C increase in GT inlet air temperature due to the increased ST output, for a given power demand. Specifically, they referred to an 80 MW CC located in Slovakia, where a waste heat source is used for controlled heating of the inlet air. Moon and Kim [8] assumed air recirculation from the outlet of compressor to its inlet to increase GT inlet temperature. This was activated in the low load regime to prevent the decrease in TIT below a specific value. The main achievement was a reduction in turndown ratio and CO emissions. Fan et al. [9] pointed out that

Turbo Expo: Turbomachinery Technical Conference & Exposition (GT2025), June 16–20, 2025. GT2025.
Manuscript received June 26, 2025; final manuscript received July 11, 2025; published online September 15, 2025. Editor: Jerzy T. Sawicki.

GT inlet air heating is more effective at low ambient temperature (T_{amb}). In particular, the optimum compressor inlet temperature (CIT) at a given gross CC output decreases as T_{amb} increases.

Gas turbine inlet conditions can also be changed by reintroducing exhaust gas at the compressor inlet, with the aim of maintaining high TOT values at low loads. Jonshagen [10] showed that a 40% recirculation rate can improve part-load η_{CC} by as much as 4.1% keeping CIT below 55 °C. The larger the benefit, the lower the load. This was confirmed in Ref. [11], where the largest gain in η_{CC} (+2.8%) was found at the minimum load (20%). Motamed et al. [12] very recently proposed a solution to enhance the part-load η_{CC} based on exhaust gas recirculation (EGR), for offshore power generation. They demonstrated a 20% and 14% increase in efficiency at part-loads for single- and two-spool gas turbine, respectively, albeit assuming a high maximum allowable CIT of 115 °C.

When EGR is integrated with IGV control, η_{CC} at part-load can be improved up to 1.2%, according to Liu and Karimi [13], while reducing CO_2 emissions and the propensity for NO_x formation. The combination of both solutions performs better than IGV considered individually, at 40–90% loads, as deduced in Ref. [14] from an energy/exergy analysis. However, the potential for performance enhancement may depend on GT characteristics. In particular, increments in η_{CC} are smaller for higher classes, such as H-class, compared to E- and F-class, due to the narrower load range of EGR action and deterioration in GT performance [15].

All of the cited studies share the goal of getting the most out of CC technology while operating at variable loads. This is in line with the current way CCs are called upon to generate power, under a flexible operating schedule to complement renewables. The well-known duck curve is not exclusive to California: it is increasingly occurring in other U.S. states and around the world, in places where the share of solar generation is increasing [16]. Flexible generation by conventional power plants, such as CCs, thus becomes even more important to meet the extreme swing in demand from mid-day to late evening, when electricity requirement is still high but solar generation has declined (Fig. 1). Indeed, with the priority given to grid stability, in some cases solar PV generation needs to be curtailed to reduce the upward slope during the evening [17]. In fact, the growth of solar and wind has been based on dispatchable energy, which is mainly dependent on NG. As an example, in 2023, new NG-fired generation capacity of 9274 MW was added to the power grid in the U.S., of which about 80% was CC plants [18]. Their capacity factor, despite being the highest in the entire CC fleet due to the latest generation GTs, was only about 66%. The contribution of CCs to the future energy landscape is also reinforced by the projected growth in global electricity demand in the coming years due to electrification in both advanced and emerging economies [19], and electricity consumption by data centers, artificial intelligence, and cryptocurrency sectors, which often run 24 h a day [20].

If flexibility solutions are a "must do" in CC plants, since most of the operation takes place at part-load and minimum load (Fig. 2), decarbonization technologies, on the other hand, are not yet

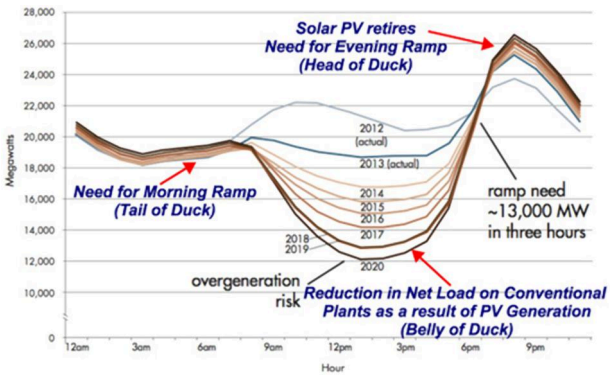

Fig. 1 Time evolution of duck curve [17]

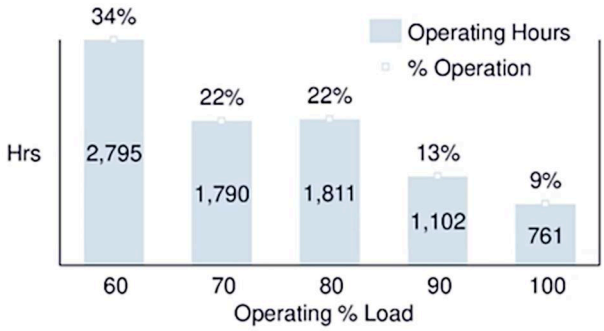

Fig. 2 Operating hours of CC power plants by load (source: Siemens Energy)

receiving sufficient support for widespread implementation, despite growing knowledge and expertise in pre- and post- removal of CO_2.

1.1 Carbon-Free Fuel. The removal of carbon from the fuel has mainly led to experimentation with hydrogen cofiring as an initial step in this direction. The shares of hydrogen vary with GT model: 44% vol for GE LM6000 [21], 20.9% vol for M501G [22], 60% vol for SGT5-4000F [23,24], and 7EA [25]. These percentages are increasing year by year and are being tested in an ever-widening GT load range: SGT-600 was shown to operate reliably with up to 60% vol hydrogen from idle to full load [26]; another GT from the same manufacturer, SGT-400, was tested in detail with a hydrogen fraction of 60%–100% vol, over a load range of 30–100% [27].

Another research topic is to retrofit existing GT to burn mixed fuels without hardware modification. For the F-class DLN combustors, very recent tests with up to 90% vol hydrogen, spanned from 30% to 100% load [28]. High-pressure, single-sector combustor testing of an FT4000 dual-fuel nozzle demonstrated successful operation on 100% hydrogen fuel with water injection, at base load [29]. For the entire GT, Harper et al. [30] documented the behavior of the SGT6-6000G, at base load, with up to 38.8% vol hydrogen: higher power output and reduced heat rate were found compared to the case with 100% NG as fuel.

In contrast, technology can be developed specifically to deal with a highly reactive fuel, such as hydrogen, and solutions differ depending on the GT manufacturer. Kawasaki established the "micromix" combustor: by combining the advantages of flashback resistance of a nonpremixed flame and dry low NO_x combustion of a premixed flame, demonstration tests were successful between 50 and 100% vol hydrogen, for the entire load range [31]. Similarly, Ansaldo has been working on the "BEV" burner, which exploits the advantages of the previous premix burners "EV" and "AEV". Multiple "BEV" burners arranged around a premix axial flow igniter make up the so-called multiburner first stage. This made it possible to use hydrogen mixtures from 10 to 100% vol under GT36 high load conditions [32]. A third-generation dry-low-emission burner was modified by Siemens to burn 100% hydrogen: the most difficult problems to address were flashback and associated damage limitations [33].

Regarding hydrogen cofiring already implemented or planned in existing or under construction NG power plants in the U.S., Table 1 shows the situation as of October 2024 [34]. Moreover, the Electric Power Research Institute (EPRI) took stock of lessons learned from demonstration projects, including:

- 45 MW GT operated by New York Power Authority, with hydrogen blends between 5% and 44% vol;
- 265 MW GT operated by Southern Company, with hydrogen shares up to 20% vol.

with the goal of outlining and sharing best practices [35].

However, the Institute for Energy Economics and Financial Analysis highlighted three significant barriers to hydrogen adoption

Table 1 Hydrogen co-firing projects in the U.S. [34]

NG power plant	GT model	%H_2 vol
De-Bary	GE 7E	100
Intermountain power Project	M501JAC	30
Magnolia	7HA.03	50
Brentwood	LM6000 PC	38
Hillabee Energy Center	SGT6-6000G	38
Orange County	M501JAC	30
Jack McDonough	M501G	20
A.J. Mihm Station	7HA.02	5

for power generation: lack of supply, lack of pipeline infrastructure, and lack of storage, as already experienced in GT blending tests [21,25–27]. In fact, on-site production of green hydrogen using 100% excess electricity from renewable sources is rarely addressed: assuming the availability of curtailed energy from solar PV and/or wind turbines, the electrolyzer and hydrogen storage should meet the needs of the specific GT, as accomplished in the HYFLEXPOWER project [27]. Nevertheless, the storage can only cover the operation of the installed GT (SGT400) at full capacity, using pure hydrogen, for one hour. With 28 h of green hydrogen testing, its availability is the limit stated by the authors.

1.2 Removal of CO_2 From the Flue Gas. To provide CO_2-free, dispatchable power, postcombustion carbon capture should be fully integrated with CC flexible operation. Among the wide range of postcombustion capture (PCC) technologies, chemical absorption with amine-based solvents is currently the most widely used on an industrial scale, offered commercially by several companies at advanced technology readiness levels of 8–9 [36]. A few modeling studies showed that part-load operation is compatible with retrofitting an existing CC with PCC [37], despite some adjustments to the capture process in terms of liquid-to-gas ratio in the absorber and specific reboiler duty (SRD) [38,39], for a GT load down to 40%.

A very recent work by GE Vernova addressed the benefits of combining PCC with EGR, but at full load [40]. First, the flue gas flowrate sent to PCC is reduced proportionally with the EGR rate, thus decreasing the size and capex of major PCC components, including the gas cooler and the absorber. Second, EGR increases the concentration of CO_2 in the exhaust gas, thus lowering the PCC technology risk. It should be remembered that the exhaust gas from industrial land-based gas turbines may contain 3–4.5% mol CO_2 at near-atmospheric pressure, depending on the GT class. Such low CO_2 concentrations/partial pressures, caused by the high levels of excess air required to reduce exhaust temperature after combustion, result in less efficient capture, higher energy penalty and larger equipment and ducts than the more established PCC experience in coal-fired power plants, where CO_2 content in the flue gas can be as high as 12–15%. Third, EGR helps to mitigate solvent degradation related to O_2 content in exhaust gas. As for the solvent, MEA is the conventional choice, but alternative blends of methyldiethanolamine and piperazine are being studied with the aim of reducing the thermal energy for the regeneration process, yet increasing the quality of the steam required [41]. Proprietary solvent formulations have also been developed with specific CO_2 capture rates and purity levels, even higher than 95% and 99.9% vol, respectively [36].

Although some studies have reported scenarios for operational flexibility of CO_2 capture plants, including variable ramp rates [42], GT startup and shutdown [43], there are no full-scale CCs with PCC in the world to the author's knowledge, and even pilot-scale PCC units to test realistic CC exhaust conditions are limited [44].

1.3 Novelty and Goals. In this study, several options for reducing carbon emissions were applied to a modern CC operating in load following mode, for given environmental conditions. The general framework and analyzed pathways, such as hydrogen cofiring, PCC and EGR, were derived from previous work [45]: each solution was implemented in the modeling platform with the aim of generating carbon-free dispatchable power with maximum efficiency. The main novelty, compared with Ref. [45], is to consider the GT control strategy at part-load as a decision variable of the optimization procedure with the CC net thermal efficiency as the objective function.

In the challenging landscape defined by the energy transition, the results can help choose the right initiatives for CC decarbonization, on a quantitative basis. Indeed, a similar approach was proposed in the literature (i.e., optimization in typical day operation schedule), but applied to a standard CC with 100% NG as fuel and no concern about the CO_2 sent to the stack, thus in a much less complex context [46,47]. While the few recent works dealing with pre- and post-CO_2 removal focus on full load [40,48], in this case, any variation in GT operating conditions may affect the downstream CO_2 capture process, thus highlighting the need for an integrated assessment of overall performance. It is specified that CO and NO_x emissions are outside the scope of this study.

2 Method and Assumptions

No changes were made to the CC layout compared to Ref. [45], in order to allow a consistent comparison of the results obtained, under different scenarios. However, for reader's convenience, a short description of both CC power block and PCC unit is provided in this section; schematic diagrams are available in under Supplemental Figs. A1–A4 available in the Supplemental Materials on the ASME Digital Collection. The optimization method is also explained to point out the original contribution of this work.

2.1 Power Block. A 2 × 1 CC was chosen as representative of a modern power plant (Fig. 3): at design point (ISO conditions), gross power ($P_{CC,g}$) and gross efficiency ($\eta_{CC,g}$) of 726.5 MW and 60.1%, respectively, refer to NG as fuel with and ideal composition of 100% CH_4 (LHV = 50047 kJ/kg). With no CO_2 capture, $P_{CC,n}$ and $\eta_{CC,n}$ decrease to 708.3 MW and 58.6%, respectively. This size is consistent with the average capacity of 2 × 1 CCs power plants built after 2015 in the U.S. [49]. The power block includes the following:

- two GE frame seven gas turbines (GE 7F.05) with hydrogen capability of up to 65% vol. The nominal gross power of each GT is $P_{GT,g} = 239$ MW, with a gross efficiency of $\eta_{GT,g} = 39.6\%$.
- one condensing ST with three sections, having a power capacity of 248.5 MW and group efficiency from 84% to 93%.

Steam is produced by recovering waste heat from the exhaust of gas turbines: each of the two heat recovery generator units has 3 pressure levels with single reheating. A water-cooled condenser completes the bottoming cycle. In the standard CC, flue gases exiting the HRSG at 81.5 °C are sent to the stack: CO_2 concentration is 4.18 vol%. Further details on the CC design point can be found in Ref. [11], Sec. 2 and Supplemental Fig. A1 available in the Supplemental Materials on the ASME Digital Collection.

Conversely, for carbon capture, flue gases pass through the PCC unit before being discharged into the environment. It consists of a quencher, an absorber and a stripper column (Fig. 4). A blower (booster-induced draft fan) is also required to compensate for the pressure drop through the CO_2-removal unit. In addition, five stages of compression with interstage cooling are needed to pressurize the captured CO_2 stream, after dehydration, to 150 bar for later utilization and/or storage. The system boundary of interest only included CO_2 compression, not its transport and storage (located in an off-site area, such as a geologic formation). The target for CO_2 removal by amine solution was set at 90%.

Steam for the reboiler comes from the ST upstream of the low-pressure section: pressure and temperature are regulated by a throttling valve and attemperator to meet the reboiler requirements (2.6 bar; 128.7 °C). The nominal SRD is 3.47 MJ/kg CO_2: this is a conservative value, given the progress toward an SRD < 3 MJ/kg CO_2. The condensate from the reboiler, at 1.6 bar (112.7 °C), is returned to the HRSG and mixed with the mainstream entering the

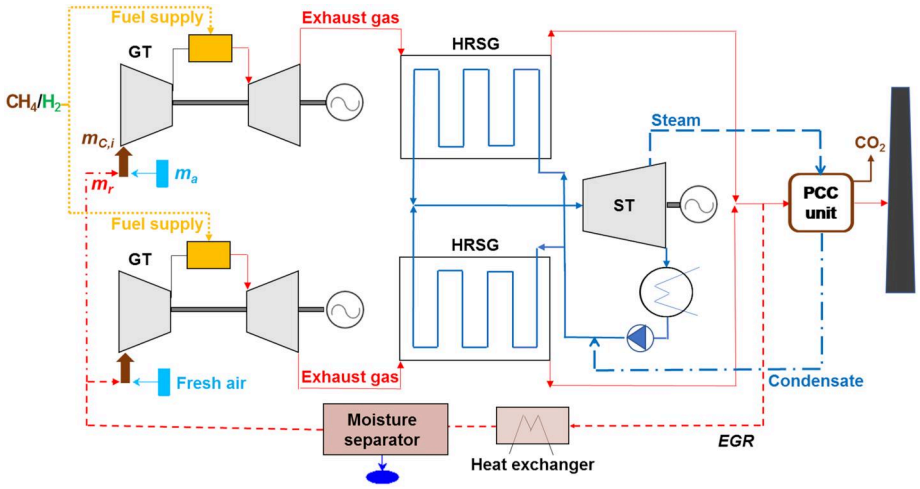

Fig. 3 Simplified layout of the power plant [45]

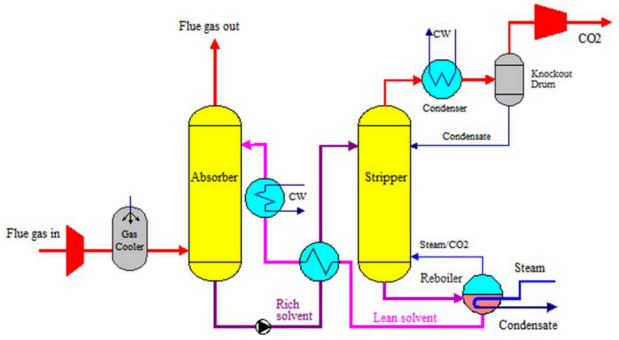

Fig. 4 Schematic process flow diagram of the PCC unit [45]

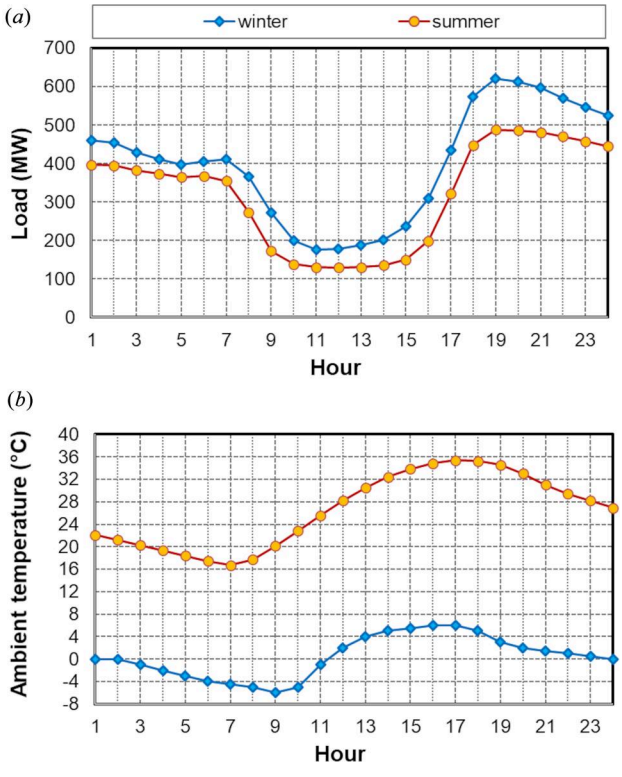

Fig. 5 Profiles of (*a*) electric load and (*b*) ambient temperature in winter and summer day [45]

first economizer. The final CO_2 concentration in the exhaust is 0.45% vol. The reader is reminded that Ref. [50] contains further information on the CO_2 capture process and its integration with the CC. It is noteworthy that the assumptions made are fully consistent with Ref. [40], which is a very recent study by a GT manufacturer (GE Vernova, Cambridge, MA).

When EGR is applied, a fraction of the flue gas recirculates in the GT intake system. Cooling and moisture removal are required before the exhaust gases are mixed with fresh air to allow the resulting flow to enter the compressor. An additional blower overcomes the pressure drop in the recirculation path. Once again, settings are in agreement with the latest theoretical and experimental investigations [48,51]. The maximum compressor inlet temperature (CIT) was defined as 54 °C. The EGR rate is the recirculated exhaust gas mass flowrate divided by the compressor inlet flowrate.

2.2 Optimization Problem: Theoretical Framework. The electricity demand profiles that the decarbonized CC must follow on an hourly basis, are shown in Fig. 5(*a*). They refer to a typical summer and winter day, characterized by the T_{amb} trend depicted in Fig. 5(*b*). They derive from a scenario outlined by the U.S. Energy Information Administration (EIA) in which the load, excluding storage, is met by a high fraction of solar power, first, then wind and hydro [52]; the residual load, net of the substantial contribution of renewables, is covered by NGCC, nuclear and coal-fired power plants, in descending order of importance and flexibility (Fig. 6). In short, the curves in Fig. 5(*a*) correspond to the blue area in Fig. 6 and extend between the minimum load of the considered CC, i.e., 20%, and the nominal capacity.

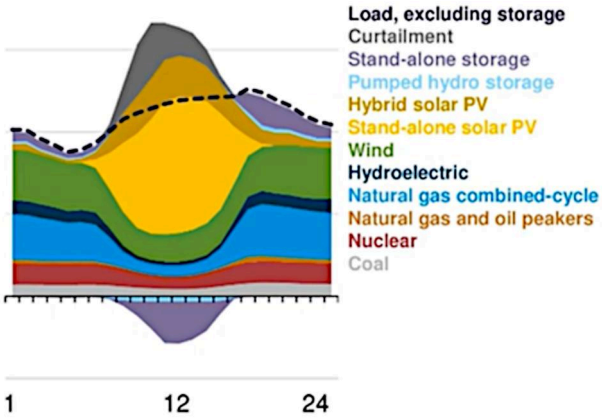

Fig. 6 Daily illustrative dispatch [52]

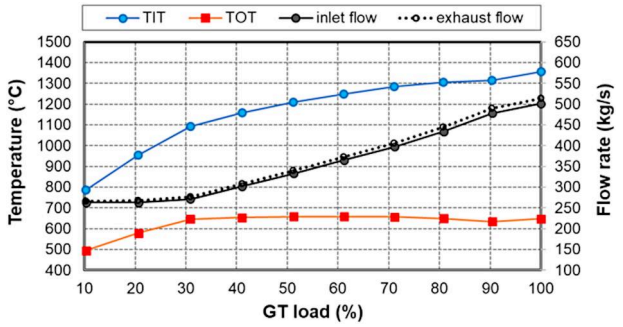

Fig. 7 Gas turbine part-load control strategy adopted in Ref. [45] (ISO conditions)

Unlike in Ref. [45], the behavior of each GT was subject to optimization, thus abandoning the strategy suggested by the manufacturer, in which TOT is maintained at the nominal level for loads within 30%, as shown in Fig. 7. In fact, TOT only drops below the rated value (648 °C) when IGV is fully closed and a further load reduction below 30% is inevitably achieved by significantly lowering the fuel input, hence TIT.

Alternatively, a user-specified partial load control was adopted in this work, based on the "XIGV" parameter available in the modeling software (Thermoflex by Thermoflow Inc. [53]). XIGV varies from 0 to 10 with the following cornerstones:

- when XIGV = 0, GT inlet airflow is kept constant whereas TIT is reduced by lowering the fuel flow. This results in decreasing TOT with load reduction;
- XIGV = 1 is associated with a reduction in the airflow and TIT/fuel to maintain TOT at its full-load value (this corresponds to Fig. 7);
- for XIGV = 10, the inlet airflow is reduced at constant TIT, thus causing an increase in TOT.

Entries of XIGV between these pivotal values led to the results illustrated on Fig. 8. It can be seen that GT inlet flow decreases with GT load: the decreasing slope becomes steeper with increasing XIGV, within $0 < \text{XIGV} \leq 10$ (Fig. 8(*a*)). The reduction of fuel input as a function of GT load confirms the linear trend, whatever the IGV value (Fig. 8(*b*)). Figure 8(*c*) shows that the part-load behavior always implies a lower TIT than the rated one (1357 °C) with a minimum of about 800 °C. The lower the GT load, the lower the TIT, with the rate of reduction increasing as XIGV decreases. But XIGV has the most significant impact on TOT, which can vary over a wide range, from 417 to 920 °C (Fig. 8(*d*)). However, there is a maximum permissible TOT that was assumed to be 700 °C within a tolerance of ±1%, i.e., about 50 °C above the nominal value [54]. It should also be noted that "XIGV = 1" is a singularity in the model, with behavior that differs significantly from that with XIGV values close to 1.

For the bottoming cycle and the PCC unit, the part-load control is set as in Ref. [45]: sliding pressure mode for the HP and IP ST stages, while for LP stage the inlet pressure is kept constant to meet the reboiler needs; the energy consumption for the capture process is a function of CO_2 concentration in the exhaust gas. In fact, SRD rises well above the design level if the CO_2 content falls below 4% vol while it slowly decreases when the amount of CO_2 exceeds this threshold.

2.3 Optimization Problem: Numerical Approach. Steady-state simulations of the decarbonized CC were performed for the following scenarios:

(1) PCC unit added to the NGCC;
(2) PCC combined with EGR in the NGCC;
(3) PCC unit added to the CC when a fuel blend with 65% vol hydrogen is used;
(4) PCC combined with EGR in the CC when the hydrogen share is 65% vol.

In all cases, the "control loop" algorithm available in Thermoflex was used to achieve the load following mode while regulating GT operation via exhaust gas temperature. Specifically, two control loops, one for each GT, were set to ensure that $P_{CC,n}$ is equal to the electric demand, within a tolerance of 0.02%. These have the GT load, between 10 and 100%, as control variable. Moreover, two additional control loops, one for each GT, were implemented to set the TOT limit at 700 °C, with "XIGV" as control variable within $0 < \text{XIGV} \leq 10$. As explained in Sec. 2.2, "XIGV" is associated with airflow modulation and fuel flow adjustment to attain the desired temperature at the GT outlet. The iterative resolution of mass and energy balances performed automatically by the code was coupled with a multivariable optimization to find the maximum $\eta_{CC,n}$. An external iterative procedure was necessary since, for a given GT load, every change in XIGV affects P_{GT}, hence $P_{CC,n}$. Therefore, a reasonable value of XIGV was chosen as a first attempt based on Fig. 8(*d*) to calculate $P_{CC,n}$. If this value turned out to be lower than the electricity demand, XIGV was reduced to allow more airflow in the GT, despite a lower TOT; conversely, XIGV was increased if the predicted $P_{CC,n}$ was higher than the load.

In cases 2 and 4, the EGR rate was also considered as a decision variable, subject to the following bounds:

- EGR rate ≤ 0.4 for case 2, to preserve flame stability with pure NG combustion [55];
- EGR rate ≤ 0.55 for case 4, to take advantage of hydrogen reactivity [56].

Indeed, the EGR rate was taken into account as an additional parameter to improve GT operational flexibility, knowing that the oxygen-depleted air entering the compressor could reduce the stoichiometric flame temperature (and thus NO_x formation). This is especially important to compensate for hydrogen combustion properties, despite the increased complexity and costs of the power plant. For a more in-depth discussion of the EGR effects on GT operation, the reader is referred to Sec. 1.3 of Ref. [45]. No need for supplemental oxygen was considered. Values of EGR rate were defined as the input of series of simulations, with a discretization step of 0.05: the procedure used the next computed values of $\eta_{CC,n}$ to guide subsequent iterations in the search for the maximum target value.

Table 2 summarizes the optimization decision variables and their constraints.

3 Results and Discussion

The results were presented following the order of the cases listed in Sec. 2.3. First, the NG-fueled CC was taken into account, with the addition of the capture process first and EGR later. Next, the mixture of hydrogen and NG was considered as fuel, in combination with residual CO_2 removal first and EGR later. Attention was drawn to the impact of the GT part-load strategy on $\eta_{CC,n}$, taking the results available in Ref. [45] as a comparison, for each case. In addition, a broader evaluation of the effectiveness of EGR was provided in the context of decarbonization under realistic operating conditions. To close the discussion, some considerations on hydrogen supply and management of captured CO_2 were added.

3.1 NGCC With Postcombustion Capture—Case 1. The lesson learnt from Ref. [45] also applies here. The decarbonized NGCC adapts its power production to fluctuations in electricity demand, ensuring the maximum $\eta_{CC,n}$, provided that one GT maintains the maximum possible capacity while the other operates at lower loads (Fig. 9(*a*)). When the demand for electricity is high enough, i.e., at night in winter day and in the late evening in summer day, GT1 works at full capacity while GT2 always works at part-load, on both days, even during peak demand (h.19). Figure 9(*b*) replicates the trend of Fig. 9(*a*) given the proportionality between GT load and $\eta_{GT,g}$, with corrections dependent on T_{amb}. Both GTs are characterized by $\eta_{GT,g}$ of less than 22% in the duck belly: the worst condition with $\eta_{GT,g} = 14\%$ refers to GT2 when the minimum load of 10% is combined with the highest T_{amb} in 10-14 time slot. In

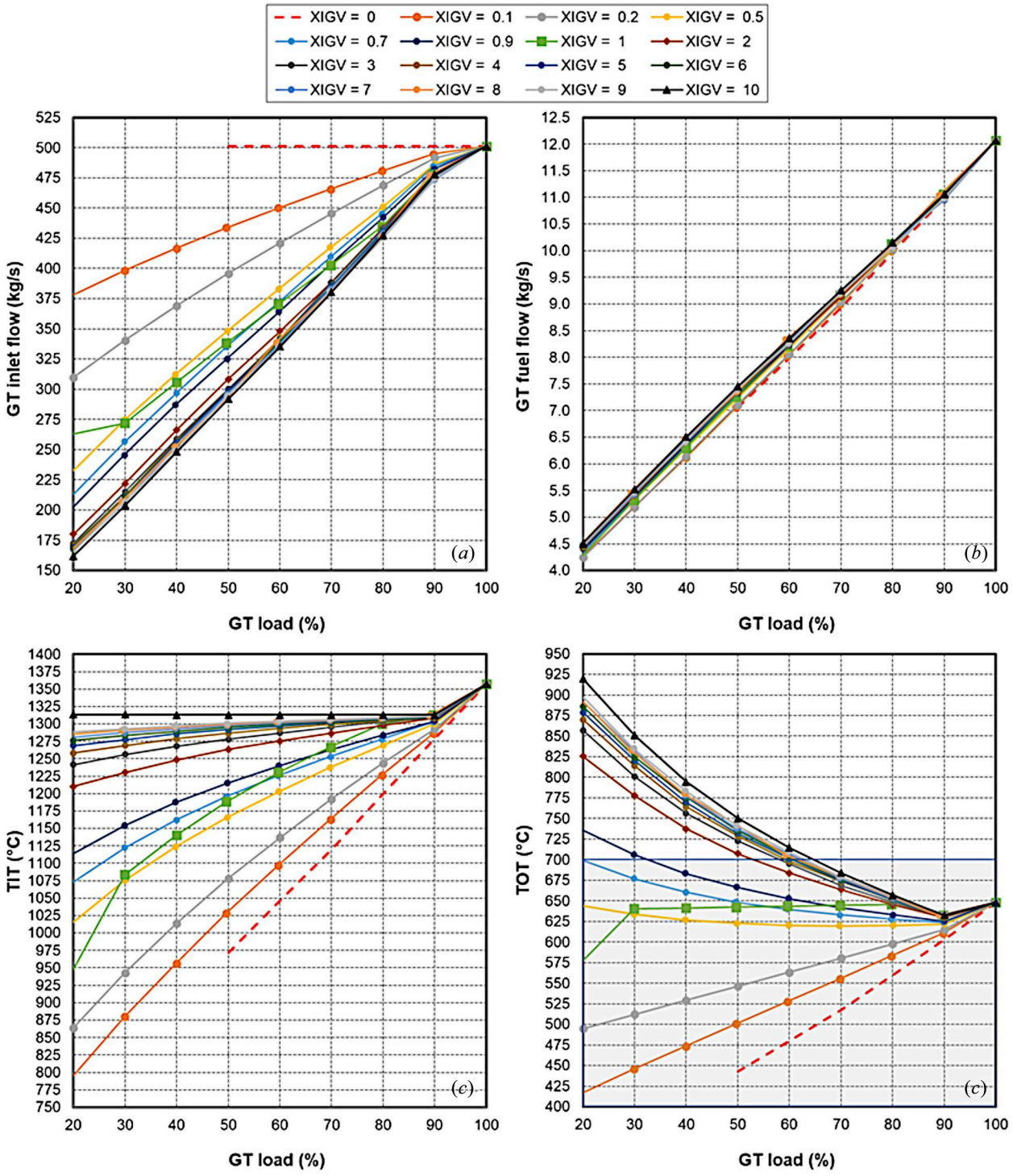

Fig. 8 Influence of "XIGV" parameter on GT part-load behavior: (*a*) inlet flow, (*b*) fuel flow, (*c*) TIT, and (*d*) TOT (ISO conditions)

Table 2 Optimization characteristics

Objective	Maximize $\eta_{CC,n}$	
Decision variables	GT1/2 load	[10–100%]
	GT1/2—XIGV	(0–10]
	GT1/2—EGR rate	(0–0.4] with 100% NG (0–0.55] with 65% vol H_2

contrast, the winter condition allows the GT1 at full load to reach $\eta_{GT,g}$ above the nominal value, around 40%. While Figure 9 does not appear to show any significant change from its counterpart in the previous work [45], it is Fig. 10 that makes the difference.

The choice of appropriate XIGV allowed TOT to rise above 680 °C, within the maximum threshold of about 705 °C, for most of the operating hours depicted in Fig. 10(*a*). Exhaust temperature values around the nominal level, with variations due to ambient conditions, are still present because associated with GT operation at full load: this is the case of GT1 during the hours 18–24, both on

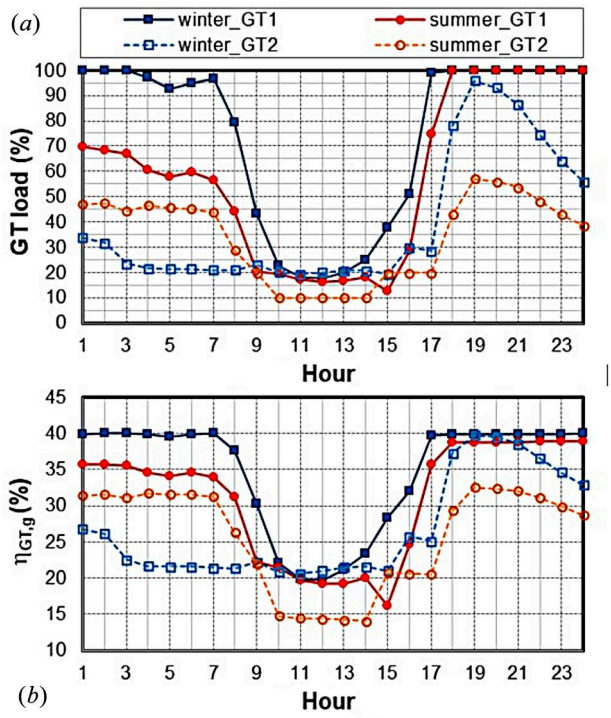

Fig. 9 Profiles of (*a*) GT load and (*b*) GT gross efficiency—case 1

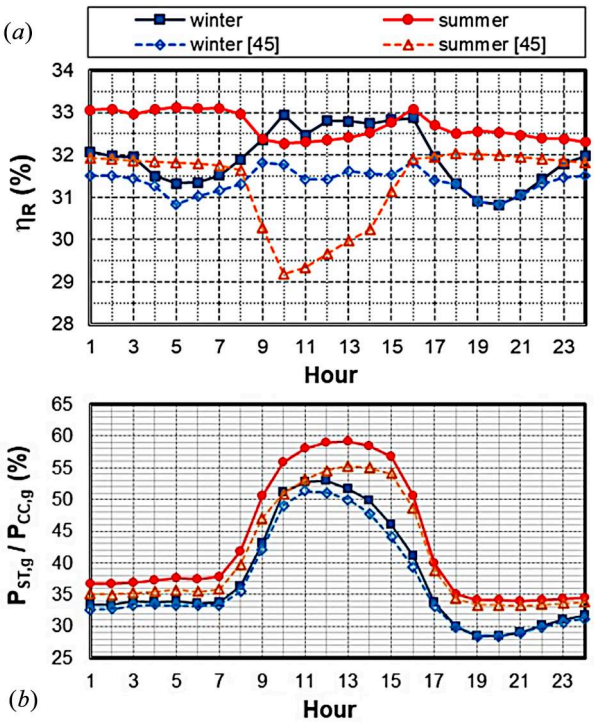

Fig. 11 Profiles of (*a*) thermal efficiency of bottoming Rankine cycle (η_R) and (*b*) ratio of ST gross power to NGCC gross power—case 1

summer and winter day. TOT slightly lower than the design point, reduced to 622 °C, is due to GT load within 90% combined with cold weather. In this case, XIGV was set to 1: in fact, Fig. 8(*d*) shows that increasing XIGV above 1 is not profitable in terms of TOT growth if the GT load is sufficiently high, i.e., above 80%. In addition, the reduction of the GT inlet flow would hamper the ability to meet the load demand.

The corresponding TIT behavior can be deduced from Fig. 10(*b*). Values above 1200 °C are maintained most of the time, even when GT load is halved. But the impact of GT control strategy is more significant at mid-day, where, although the GT load does not exceed 20%, TIT is still relatively high. Focusing on the extreme GT2 load condition, TIT varies around 990 °C from h. 10–14, which is at least 100 °C greater than the results attained in Ref. [45].

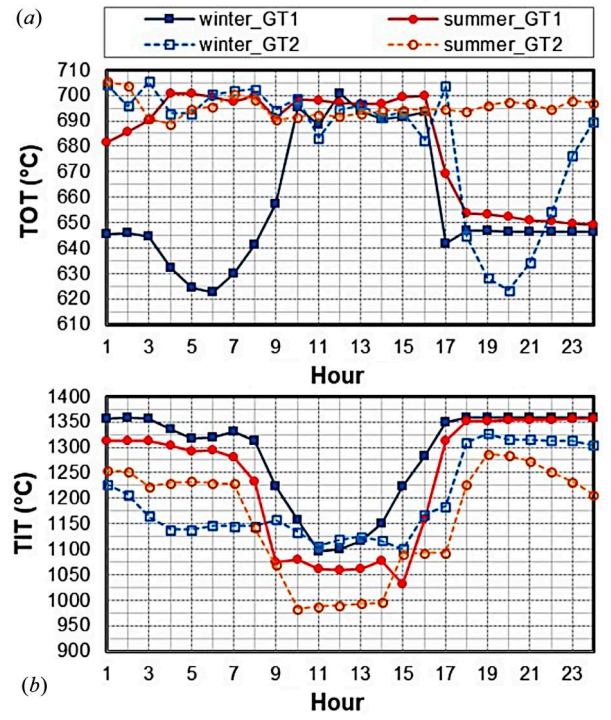

Fig. 10 Profiles of GT (*a*) TOT and (*b*) TIT—case 1

The bottoming cycle is also profoundly affected by the part-load GT control, in a positive way, because the flue gas entering the HRSG is not only hotter but also reduced in flowrate. This promotes heat recovery (Fig. 11(*a*)): in fact, η_R is always higher than that found in Ref. [45], except for a few hours when both GTs reach a very high load (from h. 18–21 in winter). The resulting gain in η_R is more significant during daylight hours: it peaks at 1.4 pp (at h. 12) and 3.1 pp (at h. 10) in winter and summer day, respectively. In the time slot 9–16, the current values of η_R, between 32.4% and 33.1%, are much greater than the corresponding $\eta_{GT,g}$ shown in Fig. 9(*b*). This reinforces the role played by the ST in energy production (Fig. 11(*b*)), contributing up to 53% in winter and 59% in summer (2 and 4 pp more than in Ref. [45]). This is consistent with what has been reported in the literature [1–3].

However, the most innovative consequences of the implemented strategy are reflected in the CO_2 capture process, which can benefit from a lower flue gas flowrate to be treated with a slightly higher CO_2 concentration (up to 0.8 pp), as a result of the XIGV setting. Hence, the total electrical power consumption of the PCC unit (P_{PCC}) is reduced, compared to Ref. [45], by up to 9% in winter and 16.5% in summer (Fig. 12).

3.2 NGCC With Postcombustion Capture and Exhaust Gas Recirculation—Case 2. A further step in this direction was taken by combining the PCC with EGR. The percentage reduction in the energy used by the capture process, compared with case 1, ranges from 17 to 35% in winter and 5 to 27% in summer (Fig. 13). This was achieved by lowering the exhaust flowrate sent to the PCC unit, in proportion to the EGR rate (see data labels). It should be clarified that the optimal EGR rate is unchanged from Ref. [45]. It is always equal to the upper limit (0.4) with the following exceptions dictated by the need to meet the grid demand:

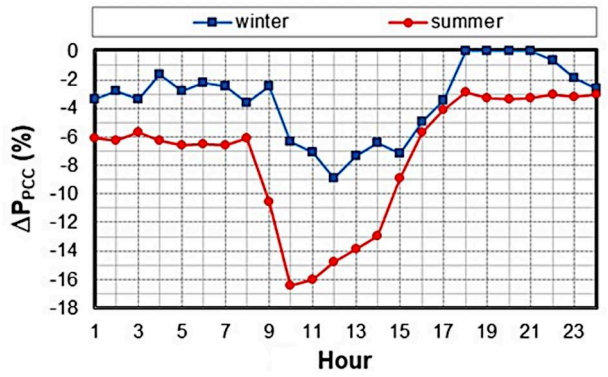

Fig. 12 Profiles of difference in PCC power consumption compared to Ref. [45]—case 1

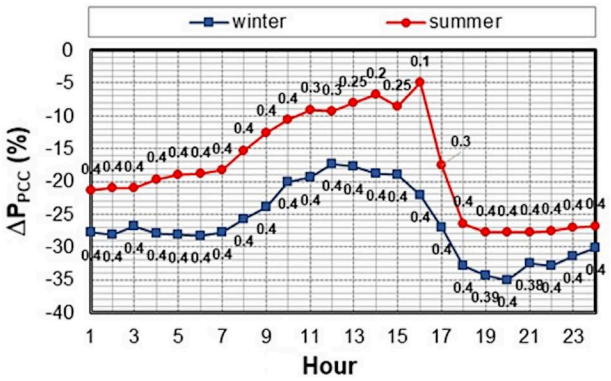

Fig. 13 Profiles of percentage reduction in PCC power consumption compared to the case without EGR (data labels show the optimal EGR rate)—case 2 versus 1

- h. 19 and 21 in winter, when it is slightly lowered to 0.39 and 0.38;
- 11–17 time slot in summer, when it is even lowered to 0.1, to compensate for the hot weather.

Moreover, CO_2 concentration in the exhaust is increased by about 2.5 ± 0.2 pp provided EGR is implemented at the highest rate of 0.4, thereby reducing SRD by about 6–8%.

As regards the effect of EGR on CC thermodynamics, the detailed dissertation provided in Ref. [50] can be summarized into the enhanced performance of the bottoming cycle. The growth in η_R, with respect to case 1, is accomplished in both days and any time (Fig. 14): it falls in the range from 0.24 and 1.35 pp, with a rather irregular pattern that also depends on the TOT resulting from the optimization. It is obvious that the smallest $\Delta\eta_R$ of 0.24 occurs at h. 16 on a summer day, due to the lowest EGR rate of 0.1.

The main outcome, i.e., $\eta_{CC,n}$, can be deduced from Fig. 15 for the cases with and without EGR (2 versus 1). Also, results from Ref. [45] were included, for the decarbonized NGCC with PCC. Load-following dynamics are evident in both days: the lowest values of $\eta_{CC,n}$ are computed at daylight hours, with the worst condition taking place in summer, while values above 47% characterize the rest of both days. On the one hand, the most efficient CC operation is provided by case 2, regardless of the day, confirming that adopting EGR is rewarding. On the other hand, the gain in $\eta_{CC,n}$ that can be obtained (compared with case 1) seems to be much more significant in winter than in summer, in agreement with Ref. [45]. In fact, it ranges from 1.2 to 2.2 pp in the cold day, while it remains below 0.9 pp throughout the hot day, with values even below 0.2 pp in summer daylight hours. In this time interval, XIGV control (in case 1) is already doing the job of boosting $\eta_{CC,n}$, as shown in Fig. 15(*b*), with a growth above the dashed line that is particularly evident from h. 10 to 14. Instead, the contribution of EGR becomes noteworthy after h. 18 as demand rises.

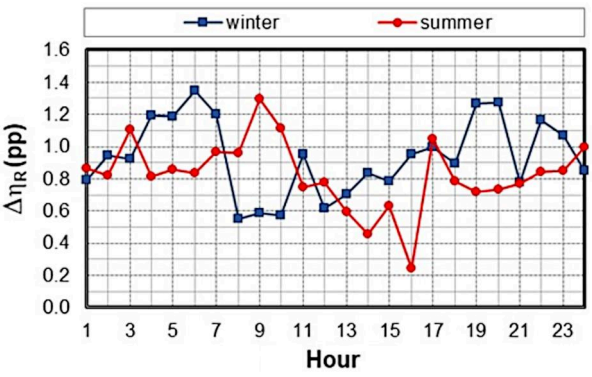

Fig. 14 Profiles of difference in bottoming Rankine cycle efficiency (η_R) compared to the case without EGR—case 2 versus 1

3.3 Combined Cycle With Hydrogen Co-Firing, Postcombustion Capture and Exhaust Gas Recirculation—Cases 3 and 4. The main effects of GT control are highlighted in Sec. 3.1 remains even when 65% of hydrogen capacity is simulated. The profiles of TOT and TIT for each GT on both days are very similar to those in Fig. 10. However, hydrogen oxidation further concentrates the exhaust energy into a reduced gas flowrate entering the HRSG, with a higher specific heat. This further promotes the bottoming cycle due to higher heat recovery and thus power production from the ST. Although profiles in Fig. 16 show roughly the same trend as in Fig. 11, greater values are attained. In fact, η_R is always higher than 33% and even above 33.5% in the mid-day hours despite extremely low loads (Fig. 16(*a*)). The largest gain in η_R, compared with Ref. [45], is 3.8 pp in summer (at h. 10) and 1.9 pp in winter (at h.11). The same is true for the fraction of $P_{CC,g}$ covered by ST (Fig. 16(*b*)): it is always above 32% but rises to a peak of 62.5% and even 70% in summer, at h. 11 and 13, respectively.

Another obvious consequence of hydrogen combustion is reducing the burden of the PCC (by at least 30% compared to case 1), whose

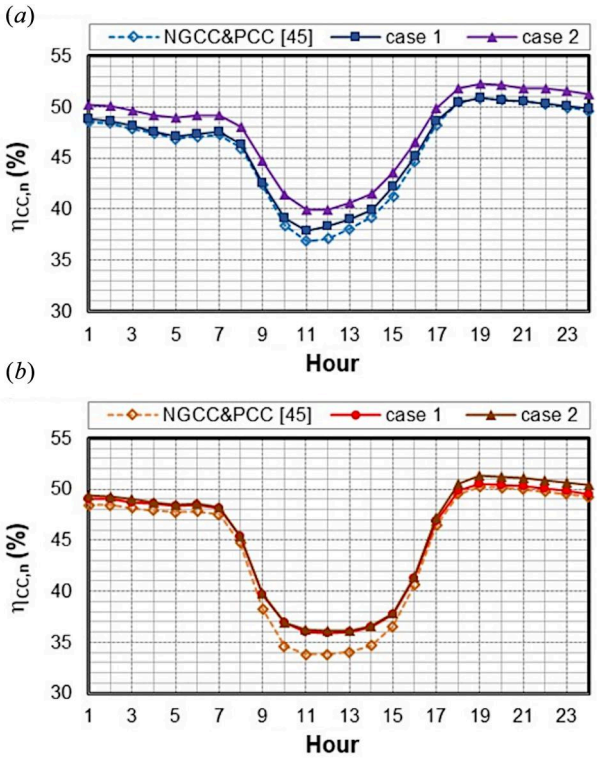

Fig. 15 Profiles of NGCC net efficiency in (*a*) winter and (*b*) summer day, with and without EGR—cases 1 and 2

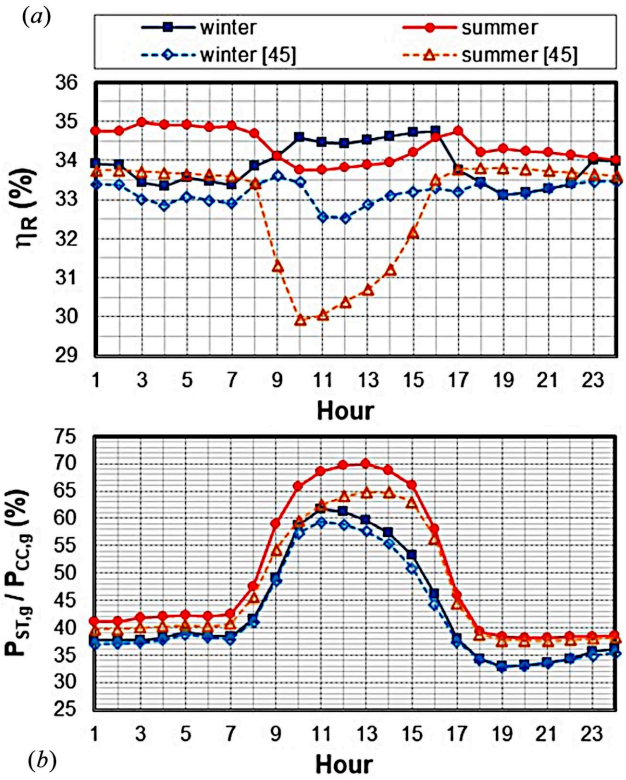

Fig. 16 Profiles of (*a*) thermal efficiency of bottoming Rankine cycle (η_R) and (*b*) ratio of ST gross power to CC gross power—case 3

energy use is expected to scale with the load, being proportional to the exhaust flowrate to being treated. But even more interestingly, XIGV control can help further reduce P_{PCC}, compared to Ref. [45], by up to 14% in winter and 22% in summer (Fig. 17). This comes from rising CO_2 content by up to 0.5 pp in a reduced amount of flue gas sent to the PCC unit. This is notable considering the very low concentration of CO_2 in the exhaust caused by the partial replacement of NG by hydrogen: it may drop to nearly 2% vol.

The subsequent addition of EGR led to the same beneficial effects discussed in Sec. 3.2, but further enhanced by higher EGR values made possible by hydrogen reactivity. Once again, the optimal EGR rate was confirmed to be the same as in Ref. [45]. Its dependence on electrical demand and environmental conditions is as follows:

- it is equal to the upper limit of 0.55 at high loads, regardless of climate;

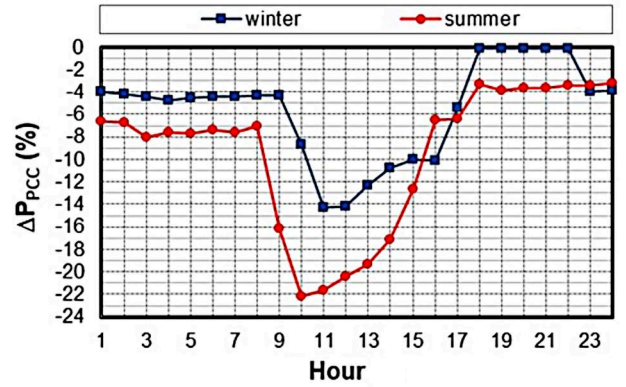

Fig. 17 Profiles of difference in PCC power consumption compared to Ref. [45]—case 3

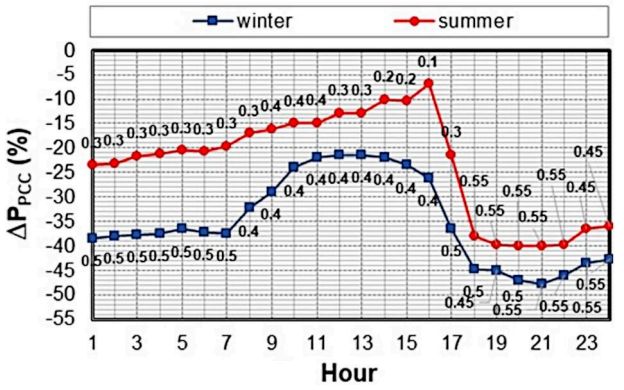

Fig. 18 Profiles of percentage reduction in PCC power consumption compared to the case without EGR (data labels show the optimal EGR rate)—case 4 versus 3

- at intermediate loads, from h.1 to 7, it is 0.5 in winter and 0.3 in summer;
- al low loads, it is stable at 0.4 in winter and decreases to 0.1 in summer to counteract warm weather.

The percentage reduction in P_{PCC}, compared with case 3, ranges from 21 to 48% in winter and 7 to 40% in summer (Fig. 18). On both days, the largest ΔP_{PCC} is obtained in the late evening, when high loads combine with the maximum EGR rate of 0.55. Furthermore, CO_2 levels in the exhaust are estimated to range between 4 and 6% vol, at EGR rate > 0.3. Accordingly, SRD decreases to nearly 15%. Moreover, the bottoming cycle gains up to 1.4 pp of η_R when EGR rate is at the upper limit.

Scenarios with hydrogen cofiring, with and without EGR (4 versus 3), were evaluated in terms of $\eta_{CC,n}$ (Fig. 19). The results of Ref. [45], related to CC with PCC, were also included. First of all, case 4 represents the best performing solution: $\eta_{CC,n}$ reaches the

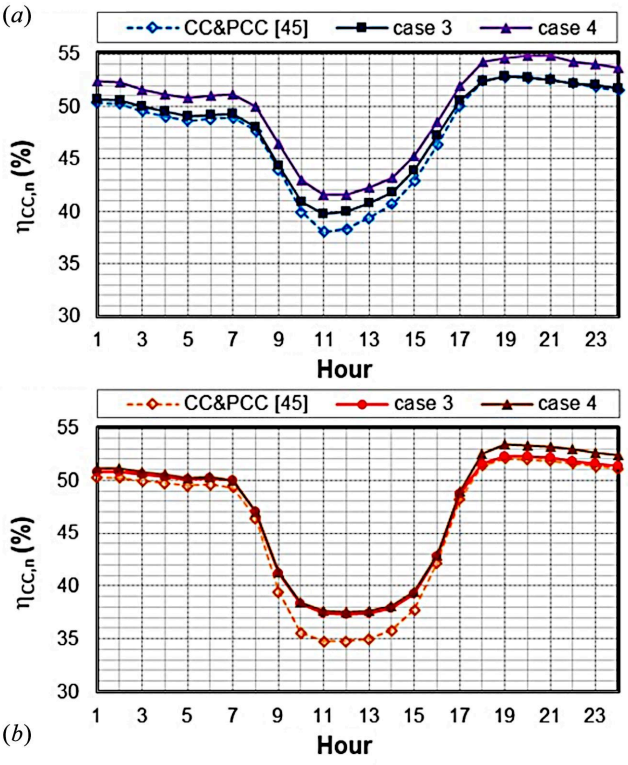

Fig. 19 Profiles of CC net efficiency in (*a*) winter and (*b*) summer day, with and without EGR—cases 3 and 4

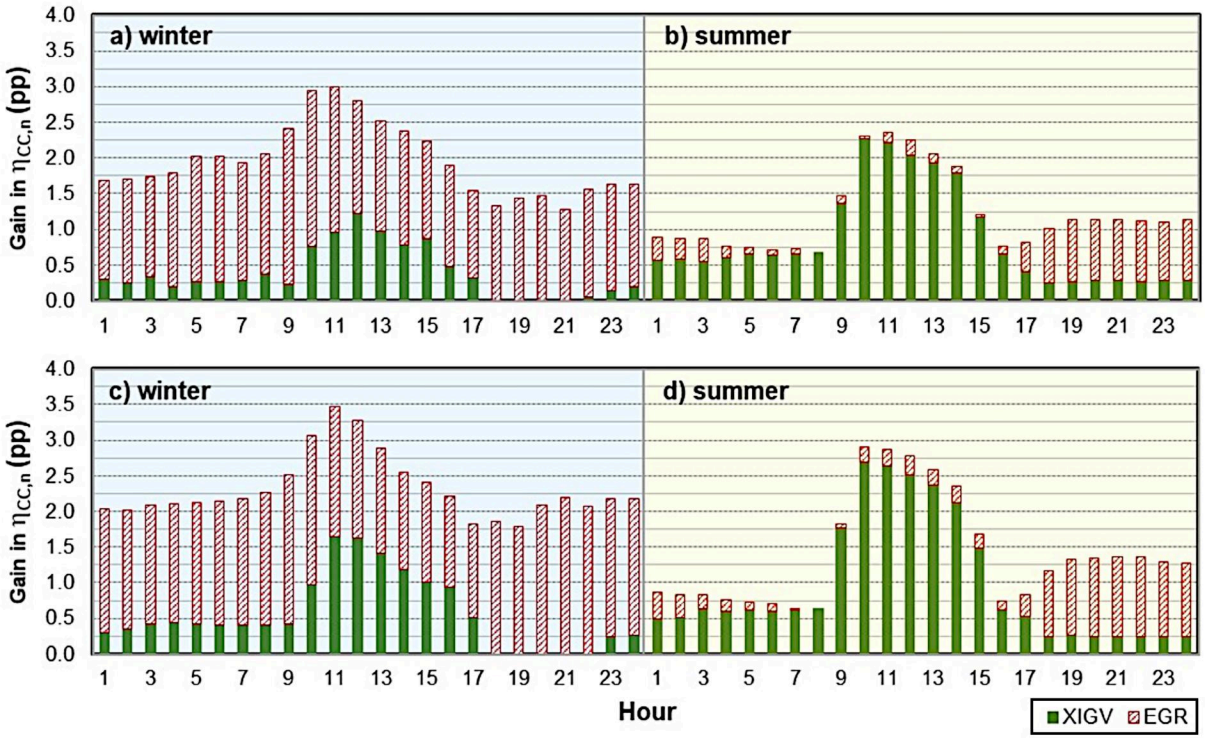

Fig. 20 Gain in $\eta_{CC,n}$ due to GT XIGV control and EGR in NGCC (top) and CCwith 65% hydrogen (bottom) for (*a* and *c*) winter (left) and (*b* and *d*) summer (right) day

highest values at h. 19–20 in both winter (54.8%) and summer (53.4%). The worst values, found around noon, of 41.5% and 37.6% in winter and summer, respectively, are almost 1.5 pp higher than the corresponding ones in case 2 (see Fig. 15). Second, it is true that combining EGR with PCC gives the best results, but the gain over case 3 is appreciable in winter but quite insignificant for most of the summer day, as already commented on Fig. 15. In fact, EGR causes an increase in $\eta_{CC,n}$ from 1.2 to 2.2 pp in the cold day, while in the hot day, an increment of around 1 pp can only be found at h. 18-24. Third, XIGV control works very well in the duck's belly, especially in summer, rising $\eta_{CC,n}$ by up to 2.7 pp around mid-day from the dashed profile.

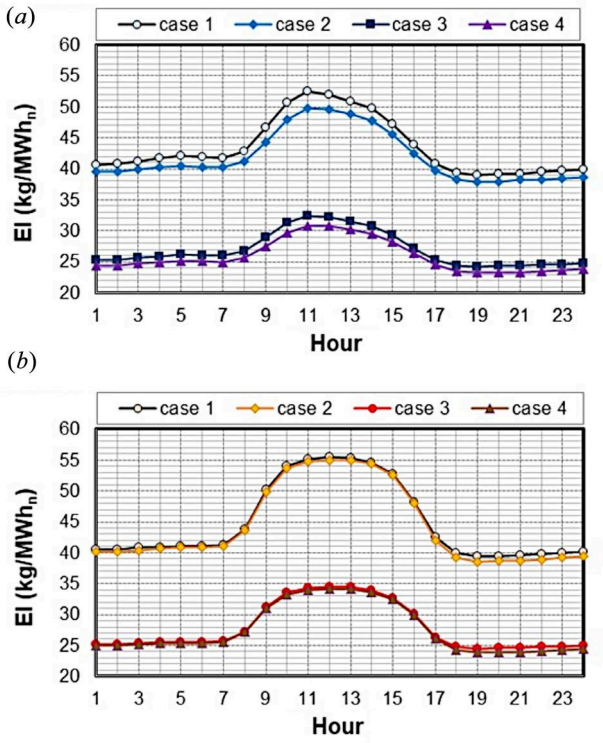

Fig. 21 Profiles of CO_2 emission intensity in (*a*) winter and (*b*) summer day—cases 1–4

3.4 Gas Turbine Control Strategy Versus Exhaust Gas Recirculation. To unveil the potential of GT regulation by XIGV and EGR in improving $\eta_{CC,n}$, the difference between the profiles in Figs. 15 and 19 were arranged in Fig. 20. The top histograms refer to the case with 100% NG as fuel while the bottom charts are inherent to the case with hydrogen cofiring. It can be inferred that the trends associated with each solution, namely, XIGV and EGR, are highly dependent on environmental conditions.

In the former case, control of GT inlet air and fuel flow gives its best at intermediate and low loads, in hot weather. Thus duck belly in the summer day represents the most suitable condition for its application, which leads to the largest gain in $\eta_{CC,n}$ of more than 2 pp. When comparing Figs. 20(*b*) and 20(*d*), with a focus on middle hours of the day, case 4 is even better than case 2 due to a reduced amount of GT exhaust resulting from hydrogen combustion.

In the latter case, EGR can be exploited to the full in cold weather, thus taking advantage of the increased CIT. On winter day, EGR brings the largest increase in $\eta_{CC,n}$ in case 4 (Fig. 20(*c*)) by applying the maximum EGR rate enabled by hydrogen. Conversely, warm weather dramatically weakens EGR, whose contribution remains quite significant only at high loads.

3.5 Final Overview. The proposed scenarios led to the CO_2 emission intensity (EI) values shown in Fig. 21. These depend on the load, being inversely related to $\eta_{CC,n}$. Therefore, all profiles show a hump during daylight hours, with the worst condition in each case occurring on the summer day. Case 4 was confirmed to provide the lowest EI, as in Ref. [45], ranging from 23 to 34 kg/MWh$_n$.

Table 3 Flue gas composition at PCC unit inlet

	Winter day		Summer day	
Mol %	CO_2	O_2	CO_2	O_2
Case 1	3.4–4.2	11.6–13.3	3.2–4.1	11.5–13.4
Case 2	5.7–6.8	5.9–8.4	3.8–6.6	5.9–11.9
Case 3	2.2–2.7	11.9–13.5	2.1–2.6	11.9–13.7
Case 4	3.6–5.8	2.0–8.9	2.4–5.6	2.3–12.3

Decarbonization due to hydrogen-enriched fuel at 65% vol is clearly evident, as EI decreases by about 38% in cases 3 and 4, compared with the corresponding cases 1 and 2, respectively. The application of EGR, regardless of fuel, resulted in a percentage reduction in EI of 2.7% and 5.6% at best in summer and winter, respectively.

In addition, the influence of EGR is felt on the composition of the exhaust gas entering the PCC unit, to an extent that depends on the optimal EGR rate. Table 3 summarizes the ranges for CO_2 and O_2 content, for each case and day. As expected, CO_2 fraction rises at the expense of O_2 content when EGR is used (cases 2 and 4), with the largest value being 6.8% and 5.8%, respectively. This is particularly important to compensate for the CO_2 dilution effect caused by hydrogen, as reflected by the lowest CO_2 percentages in case 3. The residual O_2 concentration is always above 5.9% when using pure NG (case 2), but the minimum threshold drops to 2% when cofiring hydrogen (case 4), at the highest possible EGR rate of 0.55. In contrast, the maximum O_2 availability is slightly higher in case 4 than in case 2, as an effect of hydrogen combustion [11]: it is 8.9% in the winter day, because the minimum EGR rate is 0.38, while it reaches 12.3% in the summer day, when the EGR rate falls down to 0.1.

It should be noted that the technical feasibility of EGR with NG as fuel has been demonstrated by GT manufacturers over the years, with rates up to 40% and CO_2 levels at the combustor outlet of about 8% vol [57–59]. Specifically, for GE-7F gas turbine model, tests confirmed the expected benefits of EGR discussed in Sec. 1.2, with an oxygen limit of about 7% vol in flue gas fed to the PCC unit [51], in line with case 2. For lower oxygen levels, such as those in case 4, the rationale is that hydrogen can mitigate the risk of flame instability and blow-out associated with elevated combustion dynamics (pressure fluctuations), provided the combustor has a flexible enough configuration, but experimental evidence is lacking (as far as the author is aware).

Pushing the GT technology to these limits would save energy consumption for CO_2 capture. As indicated in Table 4, case 4 has the smallest P_{PCC}, with the upper end of the range much lower than case 3, due to EGR, for roughly the same amount of CO_2 captured. Compared with case 2, the reduction in P_{PCC} is significant, ranging from 33% to 46%, despite the higher SRD values caused by CO_2 dilution due to hydrogen cofiring.

Focusing on case 4, the documented results in terms of highest $\eta_{CC,n}$ and lowest EI come from hydrogen supply, with flow rates between 1.03 and 3.37 kg/s. Depending on the primary energy and production pathway, Table 5 roughly estimates the carbon footprint of hydrogen at consumption gate. When fossil fuels are used, upstream and midstream emissions are included in addition to direct emissions, as recommended by the International Partnership for Hydrogen and Fuel Cells in the Economy [60]. It was verified that CO_2 emissions due to hydrogen supply do not exceed the CO_2 savings of case 4 provided that carbon capture is applied to the production process, be it steam methane reforming or coal gasification.

Table 5 Carbon footprint of hydrogen production pathways [60]

H_2 production route	CO_2 emission index kg CO_2-eq/kg H_2
Green hydrogen	0
Unabated NG	10–14
NG with 90% capture	0.8–6
Unabated coal gasification	23–26
Coal gasification with 90% capture	3–6

On the other hand, the captured CO_2 at high pressure is available for the next steps, i.e., transport and storage at an appropriate site. The point is that the entire CO_2 chain must not cause more emissions than it stores. Given the little operational experience, the life cycle assessment proposed by Burger et al. [61] was taken as a reference. Under the assumptions of:

- amine-based capture process with 90% capture rate (as in this study),
- CO_2 compression and conditioning to remove impurities (water and oxygen),
- temporary storage at the emitter site and loading to standardized cargo container,
- batch-wise transport to the permanent storage by ships, barges, trains, and trucks, the climate benefit was confirmed for all cases, since the overall CO_2 avoidance efficiency lies between 50 and 70%.

4 Conclusion

Steady-state, thermodynamic simulations of a realistic 2 × 1 CC operating in a load-following mode were performed to maximize net thermal efficiency when applying different decarbonization solutions based on PCC, EGR and hydrogen-cofiring. The considered scenarios included the addition of PCC with/without EGR, with standard (100% NG) or hydrogen-enriched (65% vol) fuel. For each GT, a part-load control strategy based on modulation of intake air and fuel flow was implemented, setting an exhaust temperature 50 °C higher than the nominal value as a target. Additional decision variables in the optimization procedure were GT load and EGR rate, with the latter limited to 0.4 and 0.55, for pure NG and hydrogen blending, respectively.

The GT control strategy succeeded in increasing TOT within the prescribed limit while meeting the electricity demand. As a result, a reduced amount of hotter exhaust gas, with higher CO_2 concentration is sent first to the HRSG and then to the PCC unit, with the following consequences:

- the bottoming Rankine cycle efficiency increases due to higher heat recovery and thus greater power production by the steam turbine;
- the power consumption of the capture process is reduced.

On the one side, the integration of EGR with PCC was confirmed to be the most efficient solution to provide clean, dispatchable power, whatever the fuel, in full agreement with Ref. [45]. On the

Table 4 Captured CO_2, energy consumption of PCC unit, and specific reboiler duty

	Winter day			Summer day		
Case	CO_2 (kg/s)	P_{PCC} (MW)	SRD (MJ/kg_{CO2})	CO_2 (kg/s)	P_{PCC} (MW)	SRD (MJ/kg_{CO2})
1	23–61	10–38	3.46–3.61	18–48	7–26	3.48–3.66
2	22–59	8–25	3.27–3.33	18–47	7–19	3.28–3.53
3	14–38	6–26	3.87–4.12	11–30	5–18	3.92–4.22
4	14–36	5–15	3.32–3.57	11–29	4–11	3.33–4.02

other hand, the beneficial effects of EGR are less significant in hot weather and become negligible when high ambient temperature is combined with low loads. Under these conditions, the proposed GT control strategy proved to be very effective in boosting $\eta_{CC,n}$ while also requiring a much simpler implementation than EGR. This is even more true in case of hydrogen cofiring.

Further research could deepen the rethinking of part-load GT control from a perspective of integration with PCC, adopting not only compressor variable inlet guide vanes but also variable area nozzles of the power turbine. In addition, GTs of different classes could be considered for inclusion in a decarbonized CC with single/double/triple pressure HRSG [62], with the understanding that the air-fuel ratio may contribute to CO_2 concentration in the exhaust, whatever the layout.

Nomenclature

EI = emission intensity, kg/J
h = enthalpy, J/kg
LHV = lower heating value, J/kg
m = mass flow rate, kg/s
p = pressure, Pa
P = power, J/s
SRD = specific reboiler duty, J/kg
T = temperature, K
vol = by volume, %
η = thermal efficiency, %

Subscripts

amb = ambient
g = gross
n = net
R = Rankine

Abbreviations

CC = combined cycle
CIT = compressor inlet temperature
DLE = dry low emission
DLN = dry low NO×
EGR = exhaust gas recirculation
EIA = Energy Information Administration
GT = gas turbine
HP = high pressure
HRSG = heat recovery steam generator
IGV = inlet guide vane
IP = intermediate pressure
LP = low pressure
MEA = mono-ethanolamine
NG = natural gas
PCC = postcombustion capture
pp = percentage points
ST = steam turbine
TIT = turbine inlet temperature
TOT = turbine outlet temperature

References

[1] Kim, T. S., 2004, "Comparative Analysis on the Part Load Performance of Combined Cycle Plants Considering Design Performance and Power Control Strategy," Energy, **29**(1), pp. 71–85.
[2] Huang, Z., Yang, C., Yang, H., and Ma, X., 2018, "Ability of Adjusting Heating/Power for Combined Cooling Heating and Power System Using Alternative Gas Turbine Operation Strategies in Combined Cycle Units," Energy Convers. Manag., **173**, pp. 271–282.
[3] Purba, O., and Zhultriza, F., 2021, "Inlet Guide Vane Tracking Effectiveness at Various Compressor Efficiency of Gas Turbine," IOP Conf. Ser.: Mater. Sci. Eng., **1096**(1), p. 012088.
[4] Wang, Z., Duan, L., and Zhang, Z., 2023, "Environmental Thermoeconomic Performance Analysis of Gas Turbine Combined Cycle Under Off-Design Conditions," Energy Sci. Eng., **11**(1), pp. 127–142.
[5] Yang, Y., Bai, Z., Zhang, G., Li, Y., Wang, Z., and Yu, G., 2019, "Design/Off-Design Performance Simulation and Discussion for the Gas Turbine Combined Cycle With Inlet Air Heating," Energy, **178**, pp. 386–399.
[6] Wang, S., Liu, Z., Cordtz, R., Imran, M., and Fu, Z., 2019, "Performance Prediction of the Combined Cycle Power Plant With Inlet Air Heating Under Part Load Conditions," Energy Convers. Manag., **200**, p. 112063.
[7] Variny, M., and Mierka, O., 2009, "Improvement of Part Load Efficiency of a Combined Cycle Power Plant Provisioning Ancillary Services," Appl. Energy , **86**(6), pp. 888–894.
[8] Moon, S. W., and Kim, T. S., 2021, "Simulation of Optimizing the Partial Load Performance of a Gas Turbine Combined Cycle Using Exhaust Heat Recuperation and Inlet Bleed Heating," ASME J. Eng. Gas Turbines Power, **143**(6), p. 061005.
[9] Fan, K., Yang, C., Xie, Z., and Ma, X., 2021, "Load-Regulation Characteristics of Gas Turbine Combined Cycle Power System Controlled With Compressor Inlet Air Heating," Appl. Therm. Eng., **196**, p. 117285.
[10] Jonshagen, K., 2016, "Exhaust Gas Recirculation to Improve Part Load Performance on Combined Cycle Power Plants," ASME Paper No. GT2016-56229.
[11] Ravelli, S., 2022, "Thermodynamic Assessment of Exhaust Gas Recirculation in High-Volume Hydrogen Gas Turbines in Combined Cycle Mode," ASME J. Eng. Gas Turbines Power, **144**(11), p. 111012.
[12] C., Motamed, M. A., Genrup, M., and Nord, L. O., 2024, "Part-Load Thermal Efficiency Enhancement in Gas Turbine Combined Cycles by Exhaust Gas Recirculation," Appl. Therm. Eng., **244**, p. 122716.
[13] Liu, Z., and Karimi, I. A., 2018, "New Operating Strategy for a Combined Cycle Gas Turbine Power Plant," Energy Convers. Manag., **171**, pp. 1675–1684.
[14] Li, K., Chi, J., and Zhang, S., 2023, "Energy and Exergy Analysis of Gas Turbine Combined Cycle With Exhaust Gas Recirculation Under Part-Load Conditions," J. Mech. Sci. Technol., **37**(5), pp. 2149–2160.
[15] Li, K., Chi, J., Wang, B., and Zhang, S., 2024, "Thermodynamic Performance Analysis of E/F/H-Class Gas Turbine Combined Cycle With Exhaust Gas Recirculation and Inlet/Variable Guide Vane Adjustment Under Part-Load Conditions," J. Therm. Sci., **33**(1), pp. 348–367.
[16] EIA, 2023, "As Solar Capacity Grows, Duck Curves Are Getting Deeper in California," EIA, Washington, DC, accessed Oct. 15, 2024, https://www.eia.gov/todayinenergy/detail.php?id=56880
[17] Ghosh, S., Roy, J. N., and Chakraborty, C., 2024, "Decarbonizing the Electricity Sector Using Terawatt-Scale Interconnected Photovoltaic Power Grids to Meet the Climate Goals: A Comprehensive Review and a Strategic Roadmap," Sol. Compass, **12**, p. 100088.
[18] EIA, 2024, "Use of Natural Gas-Fired Generation Differs in the United States by Technology and Region," EIA, Washington, DC, accessed Oct. 22, 2024, https://www.eia.gov/todayinenergy/detail.php?id=61444
[19] EIA, 2024, "Electricity Mid-Year Update," IEA, Paris, France, accessed Oct. 30, 2024, https://www.iea.org/reports/electricity-mid-year-update-july-2024
[20] Davenport, C., Singer, C. F. A., Mehta, N., Lee, B., Mackay, J., Modak, A., Corbett, B., et al., 2024, "AI, Data Centers and the Coming U.S. Power Demand Surge," Goldman Sachs, New York, accessed Oct. 24, 2024, https://www.spirepointpc.com/documents/FG/spirepoint/resource-center/629373_Generational_Growth__AI_data_centers_and_the_coming_US_power_demand_surge.pdf
[21] Steele, R. C., Martz, T. D., Ettlinger, A., Zandes, T., Alexander, M. J., Hockman, B. K., and Goldmeer, J., 2023, "Hydrogen Co-Firing Demonstration at New York Power Authority Brentwood Site: GE LM6000 Gas Turbine," ASME Paper No. GT2023-101283.
[22] Harper, J., Cloyd, S., Pigon, T., Thomas, B., Wilson, J., Johnson, E., and Noble, D. R., 2023, "Hydrogen Co-Firing Demonstration at Georgia Power's Plant McDonough: M501G Gas Turbine," ASME Paper No. GT2023-102660.
[23] Blaette, L., Schmitz, U., Streb, H., and Vogtmann, D., 2023, "SGT5-4000F Hydrogen Capability–High Pressure Combustion Rig Tests," ASME Paper No. GT2023-103574.
[24] Blätte, L., Goeb, D., Gruhlke, P., Prade, B., Schildmacher, K. U., Streb, H., and Vogtmann, D., 2024, "SGT5-4000F Hydrogen Capability–High Pressure Combustion Rig Tests Part II," ASME Paper No. GT2024-123364.
[25] Demougeot, N., Bullard, T., Kalb, B., Hernandez, F., Spalding, M., Yaquinto, M., Soffritti, G., van den Hout, F., Lee, D. K., and Hwang, J. W., 2024, "Heavy Duty H_2 Gas Turbine Demonstration - A Combined Experience," ASME Paper No. GT2024-126848.
[26] Berg, A., and Magnusson, R., 2023, "Fleet Experience of SGT-600 (24 MW) DLE Gas Turbine With Over 60% H_2 in Natural Gas," ASME Paper No. GT2023-103650.
[27] Parsania, N., Hermeth, S., Witzel, B., Yilmaz, E., Fourcade, S., Garmadi, S., Trump, H., and McCaig, P., 2024, "HYFLEXPOWER Project: Demonstration of an Industrial Power-to-H_2-to-Power Advanced Plant Concept With Up to 100% H_2 in an SGT-400 Gas Turbine," ASME Paper No. GT2024-124016.
[28] Lee, S., Park, J., Park, S., Choi, N., and Shin, J., 2024, "Experimental Study of Natural Gas and Hydrogen Cofiring Characteristics Using Different Types of Single Nozzles of F-Class Practical Gas Turbine Combustors," ASME J. Eng. Gas Turbines Power, **146**(12), p. 121017.
[29] Locke, J., Kim, W., Smith, L., Snyder, T., and Dayton, J., 2024, "Operation of FT4000® Single Nozzle Combustor With High Hydrogen," ASME Paper No. GT2024-121321.
[30] Harper, J., Gibeaut, D., Lozier, M., Sake, R., Wolf, T., and Noble, D. R., 2024, "Hydrogen Co-Firing Demonstration at Constellation Hillabee Siemens Energy SGT6-6000 g Power Plant," ASME J. Eng. Gas Turbines Power, **147**(5), p. 051025.
[31] Aoki, S., Uto, T., Takahashi, N., Okada, K., Kroniger, D., Kamiya, H., Yamaguchi, M., et al., 2024, "Development of Hydrogen and Micromix Combustor for Small and Medium Size Gas Turbine of Kawasaki," ASME Paper No. GT2024-121073.
[32] Pennell, D., Tay-Wo-Chong, L., Smith, R., Sierra Sanchez, P., and Ciani, A., 2023, "GT36 First Stage Development Enabling Load and Fuel (H_2) Flexibility With Low Emissions," ASME Paper No. GT2023-103568.

[33] Hermeth, S., Panek, L., Witzel, B., Grandt, C., Koestlin, B., Wanjura, S., Teuber, H., et al., 2024, "100% H_2 DLE Gas Turbine Combustion Technology Platform Development," ASME Paper No. GT2024-128517.
[34] Patel, S., 2024, "The BIG PICTURE: Hydrogen Cofiring at U.S. Gas Power Plants (Infographic)," POWER Magazine, Rockville, MD, accessed Nov. 3, 2024, https://www.powermag.com/the-big-picture-hydrogen-cofiring-at-u-s-gas-power-plants-infographic/
[35] EPRI, 2023, "Safety and Environmental Lessons From Hydrogen-Natural Gas Cofiring Demonstrations," EPRI, Palo Alto, CA, Report No. 3002028335.
[36] Rezaei, S., Liu, A., and Hovington, P., 2023, "Emerging Technologies in Post-Combustion Carbon Dioxide Capture & Removal," Catal. Today, **423**, p. 114286.
[37] Rezazadeh, F., Gale, W. F., Hughes, K. J., and Pourkashanian, M., 2015, "Performance Viability of a Natural Gas Fired Combined Cycle Power Plant Integrated With Post-Combustion CO_2 Capture at Part-Load and Temporary Non-Capture Operations," Int. J. Greenhouse Gas Control, **39**, pp. 397–406.
[38] Oh, S. Y., and Kim, J. K., 2018, "Operational Optimization for Part-Load Performance of Amine-Based Post-Combustion CO_2 Capture Processes," Energy, **146**, pp. 57–66.
[39] Verhaeghe, A., Dubois, L., Bricteux, L., Thomas, D., Blondeau, J., and De Paepe, W., 2023, "Carbon Capture Performance Assessment Applied to Combined Cycle Gas Turbine Under Part-Load Operation," ASME J. Eng. Gas Turbines Power, **145**(4), p. 041009.
[40] Sammak, M., Smith, R., Kulkarni, P., Ravi, N., and Sholes, J., 2024, "Gas Turbine Combined Cycle System Integration With Carbon Capture Plant for Improved Value," ASME Paper No. GT2024-124227
[41] Verhaeghe, A., Bricteux, L., Demeyer, F., Blondeau, J., and De Paepe, W., 2024, "Retrofitting an Existing Combined Cycle Gas Turbine With Post-Combustion Carbon Capture: Assessment of Solvent Selection Impact on Performance," ASME Paper No. GT2024-125053.
[42] Bui, M., Fløy, N. E., de Cazenove, T., and Mac Dowell, N., 2020, "Demonstrating Flexible Operation of the Technology Centre Mongstad (TCM) CO_2 Capture Plant," Int. J. Greenhouse Gas Control, **93**, p. 102879.
[43] Tait, P., Buschle, B., Ausner, I., Valluri, P., Wehrli, M., and Lucquiaud, M., 2016, "A Pilot-Scale Study of Dynamic Response Scenarios for the Flexible Operation of Post-Combustion CO_2 Capture," Int. J. Greenhouse Gas Control, **48**, pp. 216–233.
[44] Nessi, E., Papadopoulos, A. I., and Seferlis, P., 2021, "A Review of Research Facilities, Pilot and Commercial Plants for Solvent-Based Post-Combustion CO_2 Capture: Packed Bed, Phase-Change and Rotating Processes," Int. J. Greenhouse Gas Control, **111**, p. 103474.
[45] Ravelli, S., 2024, "Thermodynamic Optimization of Load-Following Operation in a Decarbonized Combined Cycle Power Plant Under Net-Zero Scenarios," ASME J. Eng. Gas Turbines Power, **146**(10), p. 101020.
[46] Chen, Y. Z., Li, Y. G., Tsoutsanis, E., Newby, M., and Zhao, X. D., 2021, "Techno-Economic Evaluation and Optimization of CCGT Power Plant: A Multi-Criteria Decision Support System," Energy Convers. Manag., **237**, p. 114107.
[47] Liu, Z., and Karimi, I. A., 2018, "Simulation and Optimization of a Combined Cycle Gas Turbine Power Plant for Part-Load Operation," Chem. Eng. Res. Des., **131**, pp. 29–40.
[48] Vantaggiato, E., Riboldi, L., Anantharaman, R., Carcasci, C., Andreini, A., Roussanaly, S., and Ditaranto, M., 2024, "Understanding the Potential and the Challenges of a NGCC Integrated With Hydrogen-Assisted EGR and CO_2 Capture," ASME Paper No. GT2024-125639.
[49] EIA, 2023, "Electric Power Annual 2022," EIA, U.S. Energy Information Administration, Washington, DC.
[50] Ravelli, S., 2023, "Reducing the Energy Penalty of Retrofit Decarbonization in Combined Cycle Power Plants," ASME J. Eng. Gas Turbines Power, **145**(12), p. 121003.
[51] GE Gas Power, 2024, "Retrofittable Advanced Combined Cycle Integration for Flexible Decarbonized Generation," GE Gas Power, Final FEED Study Report, Report No. DE-FE0032131, accessed Nov. 14, 2024, https://www.osti.gov/servlets/purl/2377996/
[52] EIA, 2023, "Annual Energy Outlook 2023," U.S. Energy Information Administration, Washington, DC, Report No. AEO2023.
[53] Thermoflow, 2024, "Thermoflex®, Version 32," Thermoflow, Jacksonville, FL, accessed Oct. 10, https://www.thermoflow.com
[54] Elmasri, M. A., 2009, *Design of Gas Turbine Combined Cycles and Cogeneration Systems*, Thermoflow, Jacksonville, FL.
[55] ElKady, A. M., Evulet, A., Brand, A., Ursin, T. P., and Lynghjem, A., 2009, "Application of Exhaust Gas Recirculation in a DLN F-Class Combustion System for Postcombustion Carbon Capture," ASME J. Eng. Gas Turbines Power, **131**(3), p. 034505.
[56] Ditaranto, M., Heggset, T., and Berstad, D., 2020, "Concept of Hydrogen Fired Gas Turbine Cycle With Exhaust Gas Recirculation: Assessment of Process Performance," Energy, **192**, p. 116646.
[57] Evulet, A. T., ELKady, A. M., Branda, A. R., and Chinn, D., 2009, "On the Performance and Operability of GE's Dry Low NOx Combustors Utilizing Exhaust Gas Recirculation for Postcombustion Carbon Capture," Energy Procedia, **1**(1), pp. 3809–3816.
[58] Sander, F., Carroni, R., Rofka, S., and Benz, E., 2011, "Flue Gas Recirculation in a Gas Turbine: Impact on Performance and Operational Behavior," ASME Paper No. GT2011-45608.
[59] Tanaka, Y., Nose, M., Nakao, M., Saitoh, K., Ito, E., and Tsukagoshi, K., 2013, "Development of Low NO_x Combustion System With EGR for 1700 C-Class Gas Turbine," Mitsubishi Heavy Industries Tech. Rev., **50**(1), pp. 1–6.
[60] Antoni, L., 2024, "Methodology for Determining the Greenhouse Gas Emissions Associated With the Production, Conditioning, and Transport of Hydrogen to Consumption Gate," IPHE, Washington, DC, accessed Feb. 5, 2025, https://www.esmap.org/sites/default/files/Presentations/2024_01_23_Webinar_IPHE.pdf
[61] Burger, J., Nöhl, J., Seiler, J., Gabrielli, P., Oeuvray, P., Becattini, V., Reyes-Lúa, A., Riboldi, L., Sansavini, G., and Bardow, A., 2024, "Environmental Impacts of Carbon Capture, Transport, and Storage Supply Chains: Status and the Way Forward," Int. J. Greenhouse Gas Control, **132**, p. 104039.
[62] Savoldelli, E., and Ravelli, S., 2024, "Evaluating the Impact of CO_2 Capture on the Operation of Combined Cycles With Different Configurations," Energies, **17**(14), p. 3501.